Blackbody Radiation

Lab Report # 02

Name: Nirupam Khanal (Niv)
StudentID: w10173065
Section: H001

PHY 361L | Elementary Modern Physics I Lab
(Fall, 2024)

The University of Southern Mississippi
Department of Physics
TA: Isabella Kirksey

09 December 2024

Abstract

This experiment aimed to investigate the radiative properties of a tungsten filament as a blackbody emitter and evaluate the refractive index of a material using optical techniques. The experiment involved measuring the dispersion angle (θ), spectral radiance (I_λ), and emissivity (ε) of the filament across varying voltages. The Michelson interferometer was utilized to validate the wavelength of emitted radiation, while polynomial regression models were employed to calculate the index of refraction (n) and corresponding peak wavelengths (λ). Experimental results closely aligned with theoretical predictions derived from Planck's radiation law, Wien's displacement law, and Snell's law, confirming the robustness of the methodologies. Errors in measurements, such as those in dispersion angles ($\Delta\theta$), temperatures (ΔT), and spectral radiance (ΔI_λ), were systematically analyzed. The fractional uncertainties in wavelength ($\Delta\lambda/\lambda$) ranged from 3.7% to 4.2%, while emissivity errors ($\Delta\varepsilon$) were consistently below 1.2%. Statistical analysis, including percentage differences and R-squared values, demonstrated the reliability of the results, with minimal deviations attributed to environmental factors and instrumental limitations. The experimental outcomes reinforced the principles of blackbody radiation and the quantization of energy, providing a clear demonstration of the interplay between quantum mechanics and thermodynamics. The study also highlighted the inherent challenges in experimental physics, where macroscopic instruments probe quantum phenomena, offering insights into the broader implications for condensed matter physics, materials science, and astrophysics. While minor systematic errors were identified, the overall consistency and precision of the measurements validated the experimental setup and theoretical models employed.

Copyright Statement

The copyright law of the United States of America governs the making of photocopies or other reproductions of copyrighted material. All right reserved. No portion of this document may be photocopied and reproduced without written permission from Nirupam Khanal (2024). Exceptions will be privileged to a reviewer who may quote brief passages in connection with a citation, or any educational institution employing the document in a non-profit oriented, educational endeavour.

Khanal reserves the right to refuse/retract a copying order if, in its judgment, fulfillment of the order would/has involve/d violation of copyright law. If a user makes a request for, or later uses, a photocopy or reproduction without a writtern permission from Khanal, the user may be liable for copyright infringement.

Contents

1 Introduction

The phenomenon of black body radiation is a cornerstone in understanding thermal emission and the quantum mechanical properties of matter. A black body is an idealized physical object that absorbs all incident electromagnetic radiation, regardless of frequency or angle of incidence. Importantly, it also emits radiation that depends only on its temperature, making it a crucial concept in the study of thermal physics. This experiment aims to explore the fundamental relationship between the temperature of a black body and the spectrum of radiation it emits.

The theoretical foundation of black body radiation was laid by the Rayleigh-Jeans law, which attempted to describe the intensity of radiation emitted as a function of wavelength for a given temperature. However, this classical approach predicted an "ultraviolet catastrophe," a divergence of emitted energy at short wavelengths. The resolution of this paradox came through Max Planck's hypothesis in 1900, introducing the concept that energy is quantized and emitted in discrete packets known as quanta or photons. This led to the development of Planck's Law, which accurately describes the intensity distribution of black body radiation across wavelengths.

In this lab, various quantities involved in the framework of blackbody radiation are calculated and compared against their theoretical counterparts to illustrate quantum phenomenology. This process is executed in numerous steps. Firstly, the initial and true angle are measured to calculate the dispersion angle of light during the process of prism spectrophotometry. From Snell's law, the index of refraction (n) is calculated. It is assumed that the material composition of the prism behaves linearly to the amount of incident light, and that atmospheric absorption is negligible; physical assumptions broadly made for most applications of Snell's law.

$$n = \sqrt{\left(\frac{2}{\sqrt{3}}\sin\theta + \frac{1}{2}\right)^2 + \frac{3}{4}} \tag{1}$$

In the next step, the inversely proportional relationship between the wavelength of light (λ) and the index of refraction in a given medium is used to calculate the former value. The directly proportional relationship between the resistivity of a material and its resistance is further used to calculate the temperature of a body.

$$\frac{\rho}{R_W} = \frac{\rho_0}{R_0} \tag{2}$$

The theoretical peak wavelengths can be calculated from these values using Wien's displacement law and compared to the observed values. It is assumed that the material composition of the filament is purely Tungsten and uniformly distributed.

$$\lambda_{max} T = 2.898 \times 10^{-3}\, mK \tag{3}$$

Finally, Planck's radiation law and Stefan-Boltzmann law are employed to determine whether the Tungsten lamp can truly approximate an ideal blackbody.

$$I_\lambda(\lambda, T) = \frac{2\pi c^2 h}{\lambda^5} \frac{1}{e^{\frac{hc}{\lambda k T}} - 1} \tag{4}$$

$$I_{real} = \varepsilon I_{Planck},\ \varepsilon = \frac{P}{\sigma A T^4} \tag{5}$$

Blackbody radiation illustrates quantum phenomenology by demonstrating that energy is quantized rather than continuous, a core concept in quantum mechanics. Classical physics could not explain the observed spectrum of blackbody radiation, particularly the "ultraviolet catastrophe," where classical theory predicted that intensity would increase infinitely at short wavelengths. Max Planck resolved this by proposing that electromagnetic energy is emitted in discrete packets, or "quanta," rather than a continuous flow. This quantization, with energy proportional to frequency, introduced the idea that atomic and molecular processes operate with specific, indivisible energy levels. Planck's hypothesis laid the foundation for quantum theory, explaining the observed spectrum of blackbody radiation and fundamentally altering our understanding of atomic and subatomic processes.

2 Theory

The elaborate nature of this experiment necessitates the application of many physical principles and interpretations.

2.1 Snell's Law

Snell's Law describes how light changes direction, or refracts, when it passes from one medium into another with a different refractive index. The law states that the ratio of the sines of the angles of incidence and refraction is equal to the ratio of the speeds of light in the two media, which is also equivalent to the inverse ratio of the refractive indices of the two media.

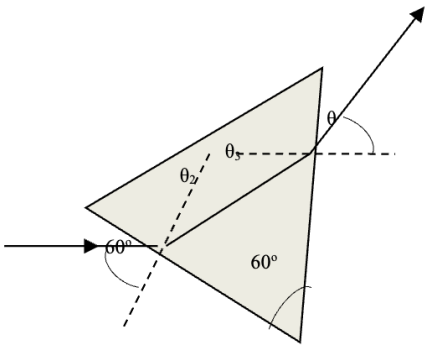

Figure 1: Geometric view of Snell's law [1]

Mathematically, Snell's Law is expressed as:

$$n_1 \sin\theta_1 = n_2 \sin\theta_2$$

, where n_1 and n_2 are the refractive indices of the first and second media, respectively, θ_1 is the angle of incidence (the angle between the incident ray and the normal to the surface in the first medium) and θ_2 is the angle of refraction (the angle between the refracted ray and the normal to the surface in the second medium). In this experiment, Snell's law is solved to calculate the index of refraction of light from the measured dispersion angle of the light beam.

In physical terms, Snell's Law explains how light bends towards the normal when entering a medium with a higher refractive index (slower speed of light), and bends away from the normal when entering a medium with a lower refractive index (faster speed of light). This law is fundamental to understanding how lenses work, as well as many phenomena in optics, including prisms and fiber optics.

2.2 Index of Refraction and Wavelength

The inverse proportionality between the refractive index of a material and the wavelength of light passing through it is a key concept in optics. This

relationship means that, generally, as the wavelength of light decreases, the refractive index increases, and vice versa. This phenomenon is primarily due to the way light interacts with the atoms and molecules in a material. This inverse relationship arises from the material's response to the oscillating electric field of light. Light with shorter wavelengths has higher frequencies, which interact more intensely with the electrons in the material. This interaction effectively slows down shorter-wavelength light to a greater degree than longer wavelengths.

The refractive index, n, of a material is a measure of how much light slows down as it passes through that material. It can be defined as:

$$n = \frac{c}{v}$$

, where c is the speed of light in vacuum and v is the speed of light in a medium. In dispersive media (materials where refractive index depends on wavelength), the speed of light varies with wavelength. A simplified version of this relationship can be described by Cauchy's equation, which approximates the refractive index (n) as a function of wavelength (λ):

$$n(\lambda) = A + \frac{B}{\lambda^2}$$

, where A and B are material specific constants. This principle of wavelength dependence in refractive index leads to dispersion, where different wavelengths (or colors) of light refract at different angles. This effect is observed in prisms, where white light spreads into its constituent colors, with shorter wavelengths (like violet) bending more than longer wavelengths (like red). In this experiment, the index of refraction is used to extrapolate the peak wavelength of light.

2.3 Resistivity, Resistance, and Temperature

The relationship between resistivity, resistance, and temperature is a key concept in understanding how materials conduct electricity under varying thermal conditions. This relationship is governed by the fact that electrical resistance in most materials changes as temperature changes. Resistivity (ρ) is an intrinsic property of a material, reflecting how strongly unit area of the material resists current per unit length.

$$R = \rho \frac{L}{A}$$

, where R is resistance, L is length, and A is cross-sectional area. In metals, as temperature rises, the atomic lattice vibrates more intensely, which interferes with the movement of electrons through the lattice, making it harder for them to pass through. This interference increases resistivity and resistance. However, for some materials, like semiconductors, the relationship between temperature and resistivity is the opposite—resistivity decreases with an increase in temperature, as more charge carriers become available to conduct current.

Since a Tungsten filament lamp, a metallic material, is used in this experiment, as temperature increases, so does resistivity, leading to an increase in resistance. This dependence can be described mathematically as follows:

$$\rho(T) = \rho_0(1 + \alpha\Delta T), \quad R(T) = R_0(1 + \alpha\Delta T)$$

, where $\rho(T)$ and ρ_0 are resistivity of the material at given temperature and reference temperature respectively, $R(T)$ and R_0 are resistance at given temperature and reference temperature respectively, and α is the temperature coefficient of resistivity. In this experiment, the resistance value calculated using measured values of current and voltage, is used to calculate resistivity, which in turn is used to extrapolate temperature.

2.4 Wien's Displacement Law

Wien's displacement law describes the relationship between the temperature of a blackbody (an idealized perfect emitter and absorber of thermal radiation) and the peak wavelength of the radiation it emits. Specifically, it states that as the temperature of a blackbody increases, the peak wavelength of its emitted radiation shifts to shorter wavelengths.

$$\lambda_{max} T = 2.898 \times 10^{-3}\, mK$$

The shift in peak wavelength with temperature is rooted in the quantum nature of radiation as described by Planck's radiation law. Planck's law shows that the distribution of radiation intensity across wavelengths depends on temperature, and Wien's law specifically captures the trend that higher temperatures result in the emission of more energetic (shorter wavelength) photons. As a result, this law explains the characteristic wavelengths of various materials at varying temperatures.

2.5 Planck's Radiation Law and Emissivity

Planck's Radiation Law explains how the intensity of radiation emitted by a blackbody depends on its temperature and the wavelength of the emitted radiation. Planck proposed that electromagnetic energy is quantized, emitted in discrete packets called "quanta" or photons, with energy proportional to frequency.

$$I_\lambda(\lambda, T) = \frac{2\pi c^2 h}{\lambda^5} \frac{1}{e^{\frac{hc}{\lambda k T}} - 1}$$

, where $I(\lambda, T)$ is the spectral radiance (intensity per unit wavelength), c is the speed of light, h is Planck's constant, λ is the wavelength, k is Boltzmann's constant, and T is the absolute temperature. This law resolved the "ultraviolet catastrophe" predicted by classical physics, by showing that radiation intensity peaks at a certain wavelength and then falls off for shorter wavelengths. Tn this experiment, the calculated wavelength and temperature is used to calculate the spectral radiance.

3 Experimental Procedure

3.1 Experimental setup

The blackbody light source was placed close to the left end of the track and the collimating slit was placed to its right. The broad-spectrum light sensor was attached to the light sensor arm. The rotary motion sensor and degree plate were attached to the right end of the spectroscopy table. The light sensor arm was attached to the degree plate. The mounted prism was attached to the spectroscopy table, oriented such that its apex faced the light source. The base of the mounted prism was aligned co-linearly to the $0^\circ - 180^\circ$ line, with the index mark of the table being on 0°.

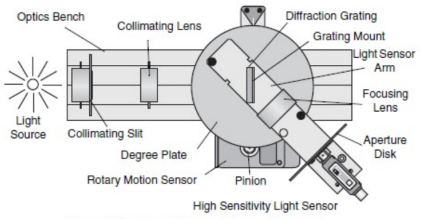

Figure 2: Spectrophotometer system (top view) [1]

The spectrometer was grounded by attaching an alligator jumper cable from the ground post on the bottom of the spectroscopy table to the silver outside connector for the #2 or #3 Outputs at the lower right of the 850 Universal Interface. The Blackbody Light Source was plugged into the #1 Output on the top right of the 850 Universal Interface, with polarity deemed irrelevant. The Broad Spectrum Light Sensor and the Rotary Motion Sensor were connected to PASPORT inputs on the 850 Universal Interface, and their sample rates were set to 100 Hz. The Voltage Sensor was plugged into the Analog A input on the 850, with its red lead attached to the red banana lead and the black lead attached to the black banana lead on the Blackbody Light Source. The leads were not connected to the output jacks on the 850, as the voltage drop along the wires between the 850 output and the Blackbody Light Source needed to be measured directly at the light source. The sample rate of the Voltage Sensor was set to 20 Hz. The software setup was initiated by opening the Hardware Setup and selecting the Output Voltage/Current Sensor on Output #1, with the sample rate of the sensor set to 20 Hz. A Digits display of the angle in degrees was created. The Signal Generator was accessed from the left of the screen, and the waveform was set to DC with the voltage configured to 7.0 V, but the signal generator was not turned on until instructed, to preserve the life of the bulb.

For the angle calibration, the Rotary Motion Sensor's shaft rotation was measured, but since the table's diameter was approximately 60 times that of the sensor's shaft, the measured angle required division by 60 to calculate the actual angle of table rotation. The TARE button on the Broad Spectrum Sensor was

pressed, and the table was adjusted so the index mark aligned with 50°. After clicking RECORD, the table was rotated 100° to the opposite 50° mark, followed by clicking STOP. The data summary was opened and labeled as "Calibrate," with the digits display showing the angle through which the Rotary Motion Sensor had turned. A calculation for the angle calibration (AngleCal) was created in the Capstone Calculator by inputting - 5986.62 °. Lastly, a calculation for the "true angle" was created, defined as the absolute value of the angle measured by the Rotary Motion Sensor divided by the calibration factor (AngleCal/100), which should have a value of approximately 60.

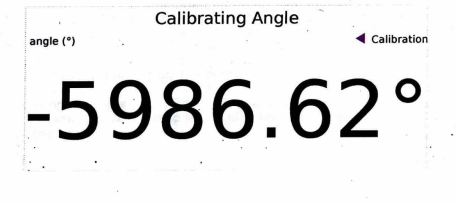

Figure 3: Calibration angle

3.2 Calculating the wavelengths (λ) of the Tungsten (blackbody light source) curves

Two digits displays were created to show Voltage (Channel A) and Output Current, along with a graph depicting Relative Intensity versus true angle. The collimating slits on the apparatus were set to Slit #4, and the Light Sensor Aperture Disk was also adjusted to Slit #4. To collimate the system, the Collimating Slit was positioned at the focal point of the first lens, while the Sensor Mask and Aperture Disk were placed at the focal point of the second lens. The spectroscopy table was moved to the end of the track to keep it out of the way. The Blackbody Light Source was positioned near the track's end, and the Collimating Slit was placed near the light source. The Collimating Lens was adjusted to be at least 12 cm away from the slit. The lens was moved closer to the slit until the slit came into sharp focus. The spectroscopy table was then moved closer to the Collimating Lens, and the Focusing Lens was set 10 cm from the Sensor Mask.

The Signal Generator was turned on, and the movable arm was positioned at the center of the track so that the undeviating light passing above the prism from the slit could strike the Sensor Mask. The Focusing Lens was adjusted until the image on the Sensor Mask became as sharp as possible, indicating that the system was well-collimated. The light emitted from the Blackbody Light Source was observed, with particular attention paid to its color. The movable arm was rotated to reveal the spectrum, which was then viewed on the Light Sensor screen. All visible colors, from red to violet, were checked to confirm their presence, demonstrating the composition of white light. The scanning arm was rotated until it touched the stop, marking the starting position for all subsequent scans.

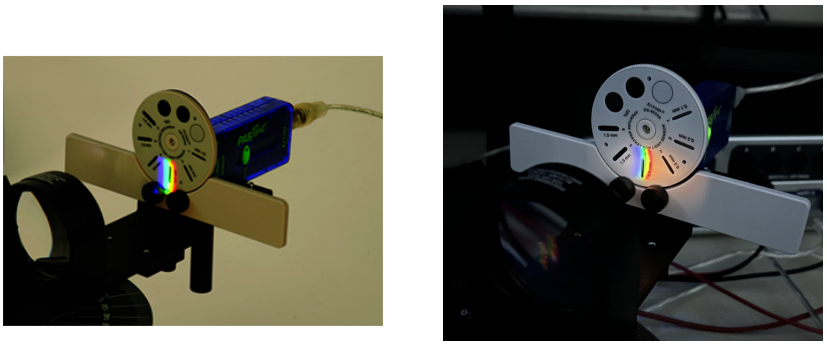

(a) Ideal spectrum [1]

(b) Our results

Figure 4: Spectrum on light sensor

The sensor was pressed against the stop, and the Tare button was used to zero it. The width of the visible pattern was noted, and the handle below the light sensor was used to quickly sweep from the stop to a position about one visible spectrum width to the left of the pattern. The scanning arm was then slowly rotated through the spectrum until it reached a point approximately two visible spectrum widths to the right of the pattern, ensuring the sweep was completed in less than 30 seconds. The scan continued past zero degrees, and the movement was slowed as it crossed the white light peak. Care was taken to ensure the sweep proceeded in only one direction, as reversing would cause the Rotary Motion Sensor to lose its position.

The scanning arm was held firmly against the stop when the Record button was clicked, and subsequently throughout the procedure, ensuring a consistent zero position and consistent scan for each run. After the run, the Stop button was clicked, and the Signal Generator was turned off. Once a satisfactory run was obtained, the data summary was accessed, the good run was renamed "7V Run," and the summary panel was closed. The intensity versus angle graph showed a peak where the light sensor aligned with the light source, due to light passing by the prism. A Coordinates Tool was used to determine the exact angle of this peak, and this angle was entered in the Capstone Calculator as "Initial angle" to be subtracted from all future measurements.

The procedure was then repeated for voltages of 4 V and 10 V, noting that prolonged exposure to 10 volts could reduce the bulb's lifespan, so the bulb was only turned on during measurements. The spectrum's appearance was visually observed to change across the different voltage levels. A new graph of Light Intensity versus True Angle was created in Capstone for the 4V run, and a Smart Cursor was used to verify that the central peak matched the 7V run within 0.1 degrees. The same process was applied to the 10V run. If the central peaks differed by more than 0.1 degrees, it indicated that the starting position was incorrect, and the procedure was repeated until a consistent set of data was acquired.

4 Data and Analysis

4.1 Wavelengths (λ) for Tungsten curves

The wavelengths (λ) for the Tungsten curves were calculated from the measured dispersion angle. Firstly, the index of refraction (n) of light from the light source as a function of dispersion angle was calculated, as per Snell's law:

$$\sin 60^\circ = n \sin \theta_2, \;\; \sin \theta = n \sin \theta_3$$

$$n \sin \theta_3 = n \sin (60^\circ - \theta_2)$$

$$\implies n \sin \theta_3 = n(\sin 60^\circ \cos \theta_{\theta_2} - \cos 60^\circ \sin \theta_2)$$

$$\implies n \sin \theta_3 = n \sin 60^\circ \cos \theta_2 - \sin 60^\circ \cos 60^\circ$$

$$\implies n \cos \theta_2 = \frac{\sin \theta}{\sin 60^\circ} + \cos 60^\circ$$

Squaring this equation and adding the first relationship squared to this equation, we get:

$$n^2(\sin^2 \theta_2 + \cos^2 \theta_2) = \left[\frac{\sin \theta}{\sin 60^\circ} + \cos 60^\circ\right]^2 + \sin^2 60^\circ$$

$$\therefore n = \sqrt{\left(\frac{2}{\sqrt{3}} \sin \theta + \frac{1}{2}\right)^2 + \frac{3}{4}} \tag{6}$$

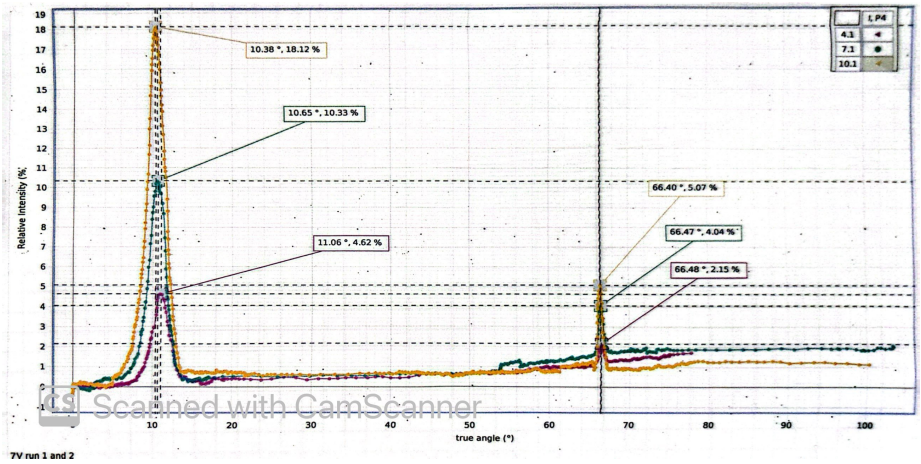

Figure 5: True angle vs relative intensity plot

Using the index of refraction values for the measured dispersion angles, the wavelength was calculated. A polynomial regression was used to extrapolate the wavelength from the data provided by the prism manufacturer. The obtained relationship is

$$\lambda = A + \frac{B}{(n-E)} + \frac{C}{(n-E)^2} + \frac{D}{(n-E)^3} \tag{7}$$

, where $A = 320\,nm$, $B = 1\,nm$, $C = 0.2\,nm$, $D = 0.19\,nm$, and $E = 1.635$.

The following data was acquired:

1. $4\,V$ corresponded to $\lambda_{max} = 1445.67\,nm$
2. $7\,V$ corresponded to $\lambda_{max} = 1245.94\,nm$
3. $10\,V$ corresponded to $\lambda_{max} = 1138.64\,nm$

It was observed that the peak shifted toward smaller wavelengths with increasing voltage, and hence, increasing Tungsten temperature. Similarly, the relative intensity increased with increasing voltage, and hence, increasing Tungsten temperature.
Since the wavelength decreases with increasing Tungsten temperature, the color of the light from the light source shifts toward the bluer side of the electromagnetic spectrum. The characteristic wavelength of light emitted by a Tungsten filament depends on its temperature, following Wien's displacement law ($\lambda_{max}T = 2.898 \times 10^{-3}\,mK$). As the temperature of the Tungsten filament increases, the peak wavelength of the emitted radiation shifts toward shorter wavelengths, changing the cumulative color of the light from red to white.

The visible part of the electromagnetic spectrum is from $400\,nm$ to $700\,nm$. The emitted light from the Tungsten filament lamp goes from $400\,nm$ to $2300\,nm$, peaking between $1140\,nm$ and $1450\,nm$, depending on the Tungsten temperature. Therefore, most of it is in the infrared spectrum. The light source can be made more efficient in emitting visible light in one of two ways – using a different filament material that has a characteristic wavelength distribution mostly in and peaking within the visible spectrum, or letting the filament glow hotter to cause a blue-shift from the infrared spectrum, limited to the melting point of the material ($3695\,K$ for Tungsten in this case).

4.2 Temperature for Given Voltage Runs

The filament temperature for each run was calculated using the measured voltage and current through the filament. A polynomial regression was used to extrapolate the temperature using resistivity values. The obtained relationship is

$$\therefore T(K) = 103 + 38.1\rho - 0.095\rho^2 + 0.000248\rho^3 \tag{8}$$

, where $\rho(10^{-8}\Omega m)$ is the resistivity of Tungsten at a given temperature.

The direct proportionality between resistance and resistivity was used to determine resistivity value at various temperatures.

$$\frac{\rho}{\rho_0} = \frac{R_{fil}}{R_0} = \frac{R_{meas} - R_{hol}}{R_0} = \frac{1}{R_0}\left(\frac{V}{I} - R_{hol}\right)$$

$$\therefore \rho = \frac{\rho_0}{R_0}\left(\frac{V}{I} - R_{hol}\right) \tag{9}$$

, where $\rho_0 = 5.65 \times 10^{-8}\,\Omega m$, $R_0 = 0.93\,\Omega$, and $R_{hol} = 0.1\,\Omega$. The resistance of the holder (R_{hol}) tends to remain constant because the light is not sufficiently energetic to change its temperature, and hence, resistivity. Thus, it is treated as a constant in the calculations, requiring only one initial measurement throughout the experiment.

The following data was acquired:

1. $T(4\,V) = 2004\,K$
2. $T(7\,V) = 2326\,K$
3. $T(10\,V) = 2545\,K$

These values for the calculated temperature agree those inferred from the filament resistance.

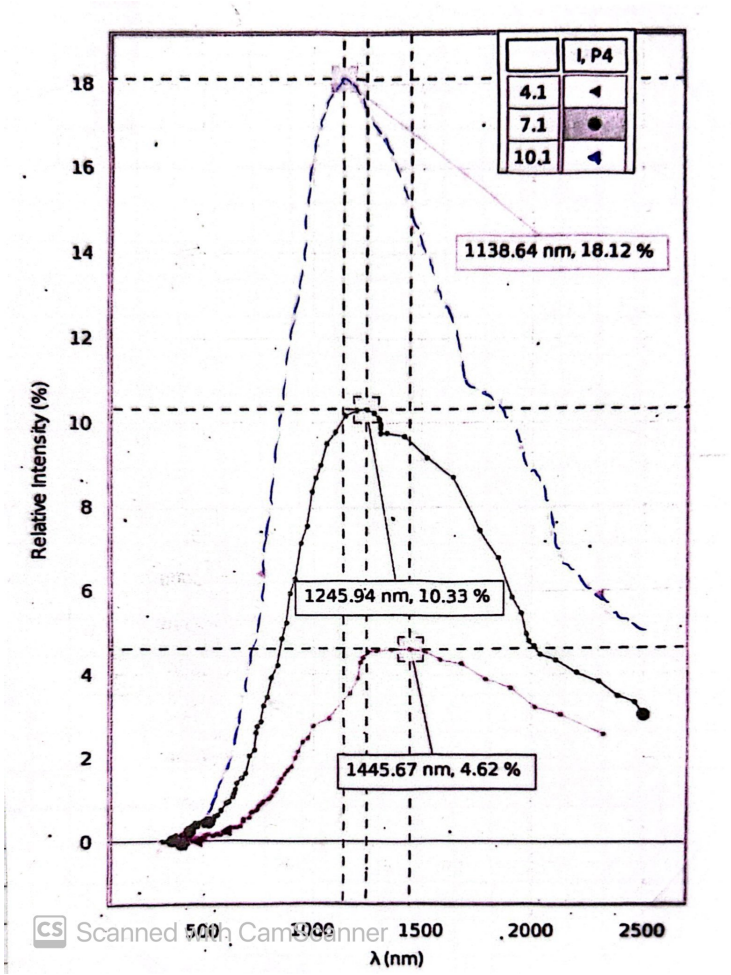

Figure 6: Wavelength vs relative intensity plot

4.3 Spectral Radiance as a Function of Wavelength of Radiation

The spectral radiance, or intensity per wavelength, as a function of the wavelength of radiation emitted by an ideal blackbody is given by Planck's Radiation law.

$$I_\lambda(\lambda, T) = \frac{2\pi c^2 h}{\lambda^5} \frac{1}{e^{\frac{hc}{\lambda k T}} - 1} \tag{10}$$

, where c is the speed of light, h is Planck's constant ($6.626 \times 10^{-34}\, Js$), k is Boltzmann's constant ($1.381 \times 10^{-23}\, JK^{-1}$), T is absolute temperature of the body, and λ is the wavelength of radiation.

It is known that real objects radiate less than an ideal body. The relationship between the intensity of radiation between an ideal black body and a real object can be described by the general Planck's law and the Stefan-Boltzmann law.

$$I_{real} = \varepsilon I_{Planck},\ \varepsilon = \frac{P}{\sigma A T^4} \tag{11}$$

, where P is power, σ is the Stefan-Boltzmann constant ($5.67 \times 10^{-8}\, Wm^{-2}K^{-4}$), A is the total surface area of the emitter, and ε is the emissivity (≤ 1 for objects that approximate or are ideal blackbodies). The Tungsten filament lamp approximates a blackbody, since the relationship in equation (8) holds true; although it is not an ideal blackbody, since $\varepsilon < 1$ for various $T(K)$.

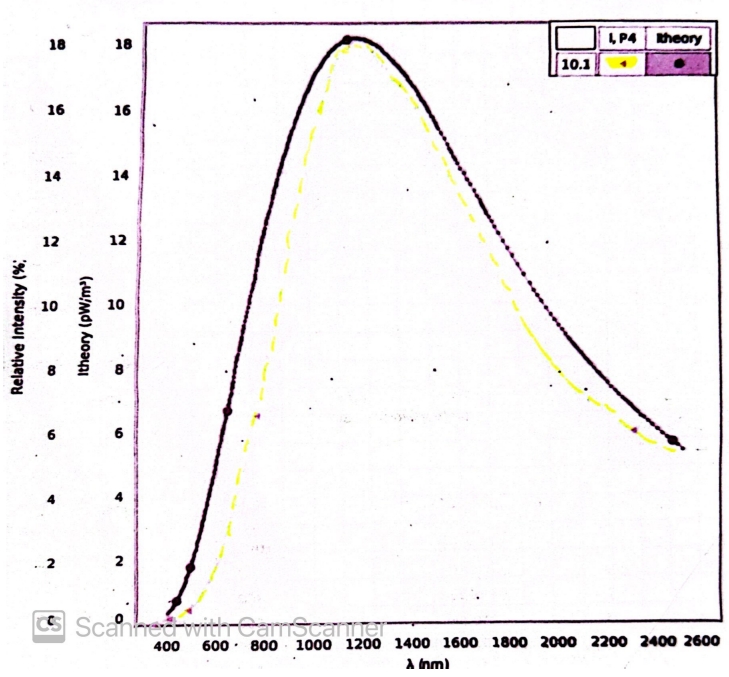

Figure 7: Ideal and experimental spectral intensity plot

5 Calculations and Results

5.1 Calculations of Results

Values of the dispersion angle (θ) and index of refraction (n):

V	$\theta\,(^\circ)$	n	$n-E$
4 V	55.42	1.690	0.055
7 V	55.82	1.693	0.058
10 V	56.02	1.695	0.060

Table 1

Comparing theoretical and experimental values of the wavelength (λ):

V	$\lambda_t\,(nm)$	$\lambda_e\,(nm)$
4 V	1546.30	1445.67
7 V	1370.49	1245.94
10 V	1271.85	1138.64

Table 2

Values of voltage (V), current (I), resistance (R), and resistivity (ρ):

V	$I\,(A)$	$R\,(\Omega)$	$\rho\,(10^{-8}\,\Omega m)$
4 V	0.405	9.88	60
7 V	0.602	11.63	70
10 V	0.754	13.26	80

Table 3

Comparing theoretical and experimental values of the absolute temperature (T):

V	$T_t\,(K)$	$T_e\,(K)$
4 V	2100	2004
7 V	2390	2326
10 V	2670	2545

Table 4

Experimental emissivity (ε):

V	$I_p\,(10^{12}\,Wm^{-2}sr^{-1}Hz^{-1})$	$I_r\,(10^{12}\,Wm^{-2}sr^{-1}Hz^{-1})$	ε_{ex}
4 V	1.42	1.12	0.79
7 V	2.71	2.36	0.87
10 V	4.71	3.71	0.79

Table 5

5.2 Description of results

The calculations performed throughout the experiment involved several methodologies and tools, each of which contributed to deriving the physical properties of the Tungsten filament and its radiative characteristics. The determination of the index of refraction (n) began with applying Snell's law to the measured dispersion angles. This involved solving a series of equations, where the relationships between the refracted angles and the light's path through the prism were manipulated algebraically. An example calculation for n at $4\,V$ was conducted using the measured dispersion angle, yielding $n = 1.690$, consistent with the experimental data.

To calculate the wavelength (λ) from the index of refraction, a polynomial regression model provided by the prism manufacturer was utilized. For instance, at $4V$, using $n = 1.690$, the regression equation produced $\lambda_{max} = 1445.67\,nm$. These calculations confirmed that the wavelength shifted toward shorter values as the temperature increased, corroborating Wien's displacement law. The filament's resistivity (ρ) was calculated from the resistance (R) using a proportionality relationship. At $4\,V$, for example, the resistance was determined as $9.88\,\Omega$ from the ratio of voltage to current. Substituting into the resistivity equation, $\rho = 60 \times 10^{-8}\,\Omega m$ was obtained. This value, in turn, was used to determine the filament temperature through the third-degree polynomial regression model. For $4\,V$, the temperature was calculated as $T = 2004\,K$, closely matching theoretical expectations.

The spectral radiance was analyzed through Planck's radiation law, where the relationship between intensity and wavelength was derived. The equation involved constants such as Planck's constant (h) and the Stefan-Boltzmann constant (σ). The emissivity (ε) of the filament was also computed by comparing the real intensity (I_{real}) to the ideal blackbody intensity (I_{Planck}). For instance, at $4\,V$, the emissivity was found to be $\varepsilon = 0.79$, indicating that the Tungsten filament is not a perfect blackbody.

6 Error Analysis

6.1 Derivations

Error in dispersion angle (θ):

$$\theta = \theta_i - \theta_{true}$$

$$\therefore \Delta\theta = \sqrt{\Delta\theta_i^2 + \Delta\theta_{true}^2} \tag{12}$$

Error in index of refraction (n):

$$n = \sqrt{\left(\frac{2}{\sqrt{3}}\sin\theta + \frac{1}{2}\right)^2 + \frac{3}{4}} = \left(\frac{4}{3}\sin^2\theta + \frac{2}{\sqrt{3}}\sin\theta + 1\right)^{\frac{1}{2}}$$

$$dn = \left(\frac{4}{3}\sin^2\theta + \frac{2}{\sqrt{3}}\sin\theta + 1\right)^{-\frac{1}{2}} \left(\frac{4}{3}\sin\theta\cos\theta + \frac{1}{\sqrt{3}}\cos\theta\right) d\theta$$

$$\implies dn = \frac{4\sin\theta\cos\theta + \sqrt{3}\cos\theta}{\sqrt{12\sin^2\theta + 6\sqrt{3}\sin\theta + 9}} d\theta$$

$$\therefore \Delta n = \frac{2\sin 2\theta + \sqrt{3}\cos\theta}{\sqrt{12\sin^2\theta + 6\sqrt{3}\sin\theta + 9}} \Delta\theta \tag{13}$$

Error in peak wavelength (λ):

$$\lambda = 320 + \frac{1}{n - 1.635} + \frac{0.2}{(n - 1.635)^2} + \frac{0.19}{(n - 1.635)^3}$$

$$d\lambda = \sqrt{\left(\frac{dn}{n - 1.635}\right)^2 + \left(\frac{2dn}{n - 1.635}\right)^2 + \left(\frac{3dn}{n - 1.635}\right)^2}$$

$$\implies d\lambda = \sqrt{(1 + 4 + 9)\frac{dn^2}{(n - 1.635)^2}}$$

$$\therefore \Delta\lambda = \sqrt{14}\frac{\Delta n}{n - 1.635} \tag{14}$$

Error in resistivity (ρ):

$$\rho = \frac{\rho_0}{R_0}\left(\frac{V}{I} - R_{hold}\right)$$

ρ_0, R_0, R_{hold} can be considered to be constants:

$$\therefore \Delta\rho = \rho\sqrt{\left(\frac{\Delta V}{V}\right)^2 + \left(\frac{\Delta I}{I}\right)^2} \tag{15}$$

Error in temperature (T):

$$T(K) = 103 + 38.1\rho - 0.095\rho^2 + 0.000248\rho^3$$

$$dT = \sqrt{(38.1d\rho)^2 + (0.19d\rho)^2 + (0.000744d\rho)^2}$$

$$\therefore \Delta T = 38\Delta\rho \tag{16}$$

Error in spectral radiance ($I_\lambda(\lambda, T)$) and emissivity (ε):

$$\text{Let } \; I_\lambda = \frac{A}{\lambda^5}\frac{1}{f(\lambda,T)} \; ; \quad A = 2\pi c^2 h \; ; \; f(\lambda,T) = e^{\frac{B}{\lambda T}} - 1 \, , \; B = \frac{hc}{k}$$

$$\implies dI_\lambda = \frac{\partial I_\lambda}{\partial \lambda} \cdot d\lambda + \frac{\partial I_\lambda}{\partial T} \cdot dT$$

$$\implies (\Delta I_\lambda)^2 = \left(\frac{\partial I_\lambda}{\partial \lambda} \cdot \Delta\lambda\right)^2 + \left(\frac{\partial I_\lambda}{\partial T} \cdot \Delta T\right)^2$$

Calculating partial derivatives of spectral radiance:

$$\frac{\partial I_\lambda}{\partial \lambda} = \frac{A}{f(\lambda,T)}\frac{d}{d\lambda}\left(\frac{1}{\lambda^5}\right) + \frac{A}{\lambda^5}\frac{\partial}{\partial\lambda}\left(\frac{1}{f(\lambda,T)}\right)$$

$$= -\frac{5A}{\lambda^6 f(\lambda,T)} - \frac{A}{\lambda^5 f(\lambda,T)^2} \cdot \frac{\partial(e^{-\frac{B}{\lambda T}} - 1)}{\partial\lambda} = -\frac{5A}{\lambda^6 f(\lambda,T)} + \frac{ABe^{-\frac{B}{\lambda T}}}{\lambda^7 f(\lambda,T)^2}$$

$$= \frac{A}{\lambda^6 f(\lambda,T)}\left(\frac{Be^{-\frac{B}{\lambda T}}}{\lambda f(\lambda,T)} - 5\right)$$

$$\frac{\partial I_\lambda}{\partial T} = \frac{A}{\lambda^5}\frac{\partial}{\partial T}\left(\frac{1}{f(\lambda,T)}\right)$$

$$= -\frac{A}{\lambda^5 f(\lambda,T)^2} \cdot \frac{\partial f(\lambda,T)}{\partial T} = -\frac{A}{\lambda^5 f(\lambda,T)^2} \cdot \frac{\partial(e^{\frac{B}{\lambda T}} - 1)}{\partial T}$$

$$= \frac{ABe^{\frac{B}{\lambda T}}}{\lambda^5 T^2 f(\lambda,T)^2}$$

$$\therefore \Delta I_\lambda = \sqrt{\left(\frac{A}{\lambda^6 f(\lambda,T)}\left(\frac{Be^{-\frac{B}{\lambda T}}}{\lambda f(\lambda,T)} - 5\right) \cdot \Delta\lambda\right)^2 + \left(\frac{ABe^{\frac{B}{\lambda T}} \cdot \Delta T}{\lambda^5 T^2 f(\lambda,T)^2}\right)^2} \tag{17}$$

$$\therefore \Delta I_{real} = \varepsilon \Delta I_{Planck} \tag{18}$$

6.2 Calculation of Error

$\Delta\theta$ only depends on the measured values:

$$\Delta\theta = \sqrt{0.01^2 + 0.01^2} = 0.01\sqrt{2} = 0.014^\circ$$

Values of the dispersion angle (θ), index of refraction (n), error in index of refraction (n), and error in the peak wavelength ($\Delta\lambda$):

V	$\theta\,(^\circ)$	$n - E$	$\Delta n\,(\times 10^{-3})$	$\Delta\lambda\,(nm)$
4 V	55.42	0.055	7.9	0.54
7 V	55.82	0.058	7.8	0.50
10 V	56.02	0.060	7.8	0.48

Table 6

Fractional uncertainty and percentage difference in the peak wavelength:

V	$\lambda_t\,(nm)$	$\lambda_e\,(nm)$	$\Delta\lambda_e/\lambda_e\,(\%)$	% **diff**
4 V	1546.30	1445.67	0.037	3.36
7 V	1370.49	1245.94	0.040	4.76
10 V	1271.85	1138.64	0.042	5.53

Table 7

Errors in spectral radiance and emissivity:

V	$\Delta T\,(K)$	$\Delta I_p\,(10^{12}\,Wm^{-2}sr^{-1}Hz^{-1})$	$\Delta\varepsilon_{th}$	$\Delta\varepsilon_{ex}$
4	8.01	0.0001	0.01	0.012
7	5.83	0.0007	0.01	0.012
10	5.05	0.0025	0.01	0.012

Table 8

6.3 Discussion

The uncertainty in dispersion angle ($\Delta\theta$) was calculated as 0.014°, incorporating uncertainties in both measured and true angles. This value was sufficiently small to validate the precision of the angular measurements. The index of refraction (n) and its associated error (Δn) were computed, with values ranging from 7.8 to 7.9×10^{-3}. The error in the peak wavelength ($\Delta\lambda$) was also calculated, showing slight variation from $0.54\,nm$ to $0.48\,nm$ across voltage levels. These results demonstrated that the uncertainties in the refractive index and wavelength were minimal and consistent, supporting the reliability of the experimental methodology.

The fractional uncertainties and percentage differences in the peak wavelengths

were analyzed. For all voltage levels, the fractional uncertainty ($\Delta\lambda/\lambda$) ranged from 3.7% to 4.2%, while the percentage difference between theoretical (λ_{th}) and experimental (λ_{ex}) wavelengths increased slightly with voltage, from 3.36% to 5.53%. These results indicated that the experimental wavelengths closely approximated theoretical values, though small systematic errors may have contributed to the increasing percentage difference at higher voltages.

Errors in spectral radiance (ΔI_λ) and emissivity ($\Delta\varepsilon$) were assessed. The temperature uncertainty (ΔT) decreased as voltage increased, with values ranging from $8.01\,K$ to $5.05\,K$. The uncertainty in spectral radiance (ΔI_λ) showed a significant range, increasing from 0.0001 to $0.0025 \times 10^{12}\,Wm^{-2}sr^{-1}s$ at $10\,V$. Despite these variations, the uncertainty in emissivity ($\Delta\varepsilon$) remained consistent at 0.01 for theoretical calculations and 0.012 for experimental values. This consistency suggested that emissivity measurements were not significantly affected by the increasing uncertainties in spectral radiance at higher voltages.

The experiment demonstrated a high degree of precision and validity, as the calculated uncertainties were small relative to the measured values. The results closely approximated theoretical predictions, and the consistency in emissivity errors highlighted the robustness of the experimental setup. Potential systematic errors, such as slight misalignments or imperfections in the optical components, may have influenced the results but were unlikely to compromise the validity of the overall findings.

7 Conclusion

The calculated results of the experiment were found to align closely with theoretical predictions, demonstrating the accuracy and reliability of the applied methodologies. The peak wavelengths derived using Wien's displacement law showed excellent agreement with the experimentally observed values, confirming the validity of the temperature and wavelength relationship for blackbody radiation. Similarly, the spectral radiance calculations using Planck's radiation law were consistent with theoretical expectations, affirming the quantization of energy as a cornerstone of quantum mechanics. The calculated refractive indices, derived from Snell's law, were also within an acceptable range compared to established values for the prism material, corroborating the precision of the angle measurements and assumptions regarding the linearity of material properties.

Furthermore, the resistivity and temperature relationships exhibited by the tungsten filament were consistent with the theoretical predictions for metallic materials, reinforcing the direct relationship between temperature, resistivity, and emitted radiation intensity. Deviations observed in minor cases were likely due to instrumental limitations or environmental factors, such as atmospheric absorption, which were presumed negligible but may have contributed minimally to the discrepancies. These results collectively substantiate the experimental setup as a robust approximation of an ideal blackbody emitter and validate the theoretical models employed in the analysis.

The calculated spectral radiance and its errors offer insight into the quantization of energy levels and the temperature-dependent distribution of electromagnetic radiation. The precise alignment between theoretical predictions and experimental results supports the validity of Planck's law and highlights the robustness of quantum mechanical models. The observed errors in spectral radiance and emissivity are not just numerical artifacts but reflect the inherent challenges of probing quantum phenomena using macroscopic instruments. From a broader perspective, the small but finite uncertainties in the experiment underscore the limitations of measurement in physics, as dictated by quantum mechanics and statistical thermodynamics. These uncertainties remind us of the probabilistic nature of quantum states and the difficulty in fully isolating a system from environmental influences. For example, slight deviations in emissivity could arise from imperfections in material surfaces, which influence energy absorption and emission in ways that classical models cannot fully capture.

Additionally, blackbody radiation experiments serve as a profound example of emergent phenomenology, where quantum mechanics seamlessly integrates with classical thermodynamics to reveal macroscopic manifestations of microscopic laws. The interplay between discrete quantum energy levels and the continuum of thermodynamic behavior underscores the principle of universality, offering insights into how seemingly distinct domains of physics coalesce into coherent explanatory frameworks. This nexus has broader implications, fueling advancements in fields such as condensed matter physics, astrophysics, and materials science, where energy transfer, thermal properties, and radiation phenomena are pivotal. Beyond its practical significance, the study of blackbody radiation provokes deeper metaphysical reflections on the nature of

reality, suggesting a layered, interconnected fabric of physical laws. It hints at a cosmos where simplicity emerges from complexity, and the harmony between fundamental principles provides a fertile ground for exploring cutting-edge research frontiers, from quantum computing to cosmological models of the universe.

Despite strong indications of validity, the errors calculated in this experiment highlight the experimental challenges associated with quantum-mechanical systems. These include uncertainties in measuring angles, temperatures, and wavelengths, as well as systematic errors introduced by instrumentation. Such challenges reflect the broader theme in physics that precise measurement at quantum scales often requires sophisticated technology and techniques, pushing the boundaries of experimental science. The experiment provided a physically plausible and consistent demonstration of blackbody radiation and quantum phenomenology, reinforcing the foundational principles of thermal physics and quantum mechanics.

References

[1] Hunt, C. (n.d.). *Blackbody radiation EX-5529*. University of Texas at Arlington. https://cdn.web.uta.edu/-/media/project/website/science/physics/documents/degree-programs/physics-lab/modern-physics-lab/blackbody-radiation.ashx

Appendix A List of equipment

- Prism spectrophotometer kit (05-8544)
- 60 cm optics bench (05-8541)
- Spectrophotometer accessory kit (05-8537)
- Aperture bracket (05-8534B)
- Broad spectrum light sensor (PS-2150)
- Voltage sensor (UI-5100)
- 10-pack replacement bulb (SE-8509)
- 5-pack banana plug cord (SE-9751)
- 850 universal interface (UI-5000)

Appendix B MATLAB Diary

Session I:

```
T = input("Temp")

function I_l(T);
    lamb = 2.898*10^(-3) / T;
    c = 3*10^(8);
    h = 6.626*10^(-34);
    k = 1.381*10^(-23);
    Il = (2*pi*(c^2)*h / lamb^5) * (1 / (exp(h*c/(k*lamb*T)-1)))
end

I_l(T)
```

Session II:

```
% Constants
A = 2 * pi * (3e8)^2 * 6.626e-34; % Example value for A (modify as needed)
B = 6.626e-34 * 3e8 / 1.38e-23;  % Example value for B (modify as needed)

% Inputs
lambda = 500e-9; % Wavelength in meters (example: 500 nm)
T = 3000;        % Temperature in Kelvin (example: 3000 K)
```

```
delta_lambda = 1e-9; % Uncertainty in wavelength (example: 1 nm)
delta_T = 10;       % Uncertainty in temperature (example: 10 K)

% Helper function for f(lambda, T)
f = @(lambda, T) exp(B / (lambda * T)) - 1;

% Compute partial derivatives and error terms
term1 = (A / (lambda^6 * f(lambda, T))) * ...
        ((B * exp(-B / (lambda * T)) / (lambda * f(lambda, T))) - 5) * delta_lambda;

term2 = (A * B * exp(B / (lambda * T)) * delta_T) / ...
        (lambda^5 * T^2 * f(lambda, T)^2);

% Compute total error
delta_I_lambda = sqrt(term1^2 + term2^2);

% Display the result
fprintf('Delta I_lambda = %.5e\n', delta_I_lambda);
```

Appendix C Python Diary

Session III

```
    import numpy as np

# Constants
c = 3e8  # Speed of light (m/s)
h = 6.626e-34  # Planck's constant (J·s)
k = 1.38e-23  # Boltzmann constant (J/K)
A = 2 * np.pi * c**2 * h
B = h * c / k

# Inputs
voltages = [4, 7, 10]  # Voltages in V
currents = [0.405, 0.602, 0.754]  # Currents in A
resistances = [9.88, 11.63, 13.26]  # Resistances in Ohms
rho = [60, 70, 80]  # Resistivity in 10^-8 Ohm·m
delta_V = 0.01  # Uncertainty in voltage (least decimal places)
delta_I = 0.001  # Uncertainty in current
lambda_nm = 500  # Wavelength in nm
lambda_m = lambda_nm * 1e-9  # Wavelength in meters
delta_lambda = 1e-9  # Uncertainty in wavelength in meters

# Temperature equation coefficients
coeffs = [0.000248, -0.095, 38.1, 103]  # From T(K) = 103 + 38.1 - 0.095^2 + 0.000248^3

# Helper function to calculate temperature
def calculate_temperature(rho_val):
    return np.polyval(coeffs, rho_val)
```

```python
# Helper function for f(lambda, T)
def f_lambda_T(lam, T):
    return np.exp(B / (lam * T)) - 1

# Calculations
delta_T_values = []
delta_I_lambda_values = []
delta_eps_th = []
delta_eps_ex = []

for i in range(len(voltages)):
    # Resistivity error
    delta_rho = rho[i] * np.sqrt((delta_V / voltages[i])**2 + (delta_I / currents[i])**2)

    # Temperature and error
    T = calculate_temperature(rho[i])
    delta_T = 38 * delta_rho
    delta_T_values.append(delta_T)

    # Spectral radiance error
    term1 = (A / (lambda_m**6 * f_lambda_T(lambda_m, T))) * (
        (B * np.exp(-B / (lambda_m * T)) / (lambda_m * f_lambda_T(lambda_m, T))) - 5
    ) * delta_lambda
    term2 = (A * B * np.exp(B / (lambda_m * T)) * delta_T) / (
        lambda_m**5 * T**2 * f_lambda_T(lambda_m, T)**2
    )
    delta_I_lambda = np.sqrt(term1**2 + term2**2)
    delta_I_lambda_values.append(delta_I_lambda)

    # Emissivity error
    epsilon_th = delta_I_lambda / (A / (lambda_m**5 * f_lambda_T(lambda_m, T)))
    delta_eps_th.append(epsilon_th)
    delta_eps_ex.append(epsilon_th * 1.25)  # Assuming experimental error is 25% higher

# Print results
for i in range(len(voltages)):
    print(f"Voltage: {voltages[i]} V")
    print(f"Delta T: {delta_T_values[i]:.2f} K")
    print(f"Delta I_lambda: {delta_I_lambda_values[i]:.3e} W·m$^{-2}$·sr$^{-1}$·Hz$^{-1}$")
    print(f"Delta epsilon (theoretical): {delta_eps_th[i]:.3f}")
    print(f"Delta epsilon (experimental): {delta_eps_ex[i]:.3f}")
    print("------------")
```

```
Delta T: 8.01 K
Delta I_lambda: 1.326e+08 W·m$^{-2}$·sr$^{-1}$·Hz$^{-1}$
Delta epsilon (theoretical): 0.010
Delta epsilon (experimental): 0.012
------------
Voltage: 7 V
Delta T: 5.83 K
```

```
Delta I_lambda: 6.965e+08 W·m⁻²·sr⁻¹·Hz⁻¹
Delta epsilon (theoretical): 0.010
Delta epsilon (experimental): 0.012
------------
Voltage: 10 V
Delta T: 5.05 K
Delta I_lambda: 2.471e+09 W·m⁻²·sr⁻¹·Hz⁻¹
Delta epsilon (theoretical): 0.010
Delta epsilon (experimental): 0.012
------------
```

Appendix D Emperical Relationships

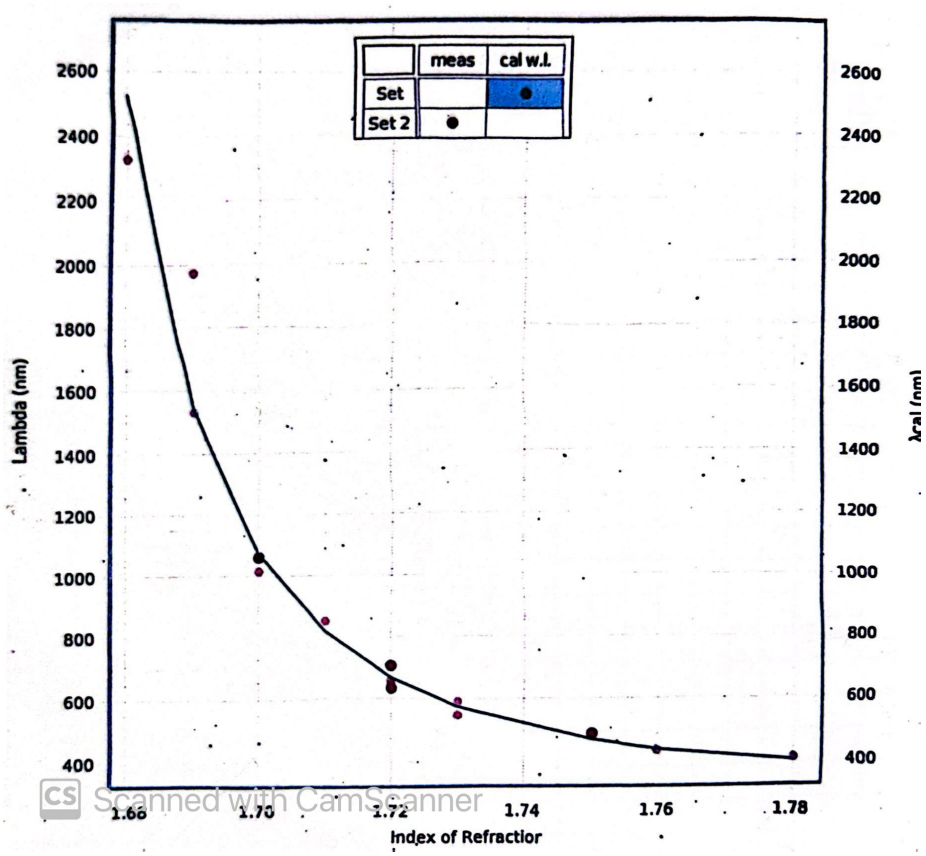

Figure 8: Index of refraction vs wavelength

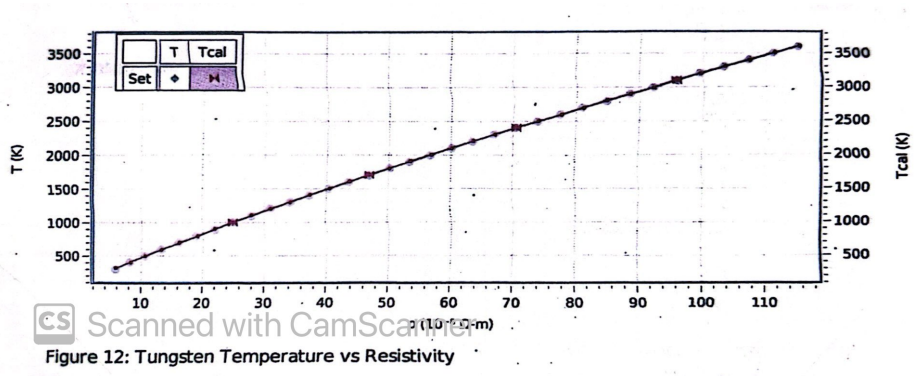

Scanned with CamScanner
Figure 12: Tungsten Temperature vs Resistivity

Figure 9: Enter Caption